Percolation in random sequential adsorption of extended objects on a triangular lattice

Lj. Budinski-Petković,[1] I. Lončarević,[1] M. Petković,[2] Z. M. Jakšić,[3] and S. B. Vrhovac[3,*]

[1]*Faculty of Engineering, Trg D. Obradovića 6, Novi Sad 21000, Serbia*

[2]*RTRK, Novi Sad 21000, Serbia*

[3]*Institute of Physics Belgrade, University of Belgrade, Pregrevica 118, Zemun 11080, Belgrade, Serbia*

(Received 3 March 2012; published 19 June 2012)

The percolation aspect of random sequential adsorption of extended objects on a triangular lattice is studied by means of Monte Carlo simulations. The depositing objects are formed by self-avoiding lattice steps on the lattice. Jamming coverage θ_{jam}, percolation threshold θ_p^*, and their ratio $\theta_p^*/\theta_{\text{jam}}$ are determined for objects of various shapes and sizes. We find that the percolation threshold θ_p^* may decrease or increase with the object size, depending on the local geometry of the objects. We demonstrate that for various objects of the same length, the threshold θ_p^* of more compact shapes exceeds the θ_p^* of elongated ones. In addition, we study polydisperse mixtures in which the size of line segments making up the mixture gradually increases with the number of components. It is found that the percolation threshold decreases, while the jamming coverage increases, with the number of components in the mixture.

DOI: 10.1103/PhysRevE.85.061117 PACS number(s): 64.60.ah, 05.10.Ln, 68.35.Rh

I. INTRODUCTION

Percolation concerns the formation of long-range connectivity in disordered systems [1] and has applications [2] in many physical, chemical, and even sociological systems [3]. Numerous practical problems include conductivity in composite materials, flow through porous media, polymerization, and behavior of scale-free random networks such as the Internet [4]. The problem of percolation is not a new one but still attracts considerable interest [5–16], and some unsolved questions remain.

In the classical site percolation model, the sites of a d-dimensional lattice are randomly occupied with probability p or remain empty with probability $1-p$. Neighboring occupied sites form a cluster. When the occupation probability is low, the occupied sites either are isolated or form very small clusters. On the other hand, for sufficiently large p a lot of occupied sites form one large cluster that reaches two opposite sides of the lattice. The lowest concentration of occupied sites for which there is a percolating cluster for an infinite lattice is called the percolation threshold.

One of the applications of percolation theory is connected to the study of physical and chemical properties of adsorbed monolayers. Irreversible adsorption of particles on solid surfaces can be successfully studied using the random sequential adsorption (RSA) model [17,18]. RSA is a process in which the objects of a specified shape are randomly and sequentially deposited onto a substrate. Excluded volume, or particle-particle interaction, is incorporated by rejection of deposition overlap, while particle-substrate interaction is modeled by the irreversibility of deposition. Once an object is placed it affects the geometry of all later placements, so the dominant effect in RSA is the blocking of the available substrate area. The deposition process ceases when all unoccupied spaces are smaller than the size of an adsorbed particle. The system is then jammed in a nonequilibrium disordered state for which the limiting (jamming) coverage θ_{jam} is less than the corresponding density of closest packing.

The interplay between RSA and percolation is relevant for description of various deposition processes and has been discussed in several works [5,6,19–21]. In Ref. [5] results for the percolation thresholds, the jamming coverages, and their ratios are given for the deposition of line segments of various lengths on a square lattice. The authors conclude that the percolation threshold is a nonmonotonic function of the line length ℓ, having a minimum due to the parallel orientation of the needles, at $\ell = 13$. The jamming coverage is found to decrease to a nonzero constant with ℓ as a power law, while the ratio of the two thresholds is nonmonotonic. However, to our knowledge, there are very few studies of such interplay for lattices other than the square lattice and for objects of various shapes.

Recently the irreversible deposition of large particles, such as polymers and nanoparticles, has attracted much attention. In Ref. [7] the temperature behavior of the percolation threshold of a system of adsorbed flexible chains on a triangular lattice was studied numerically. The flexibility of chains was controlled by the temperature via the Boltzmann factor. It was found that for the cold regime system characteristics coincide with those of straight lines. For moderate temperatures the percolation threshold drops significantly, attains a minimum at the temperature unique for all chain lengths, and grows monotonically up to an infinite-temperature limit (self-avoiding random walk case). The impact of the composition of flexible chains on the percolation properties was discussed in Ref. [8] for both the square and the triangular lattice. Simulations were performed for various chain lengths and the most favorable compositions (for which the percolation threshold acquires its minimal values) were identified. For longer and more bent chains, a no-percolating regime was detected.

Polydispersity is a common feature of real physical systems. Irreversible deposition in polydisperse systems was studied for binary mixtures [22,23], for mixtures of particles obeying various size distributions [24,25], and for polydisperse mixtures [26]. In Ref. [14] an approximate analytical approach is

*vrhovac@ipb.ac.rs; http://www.ipb.ac.rs/~vrhovac/

TABLE I. (Color online) Jamming coverage $\theta_{\text{jam}}^{(x)}$ and percolation threshold $\theta_p^{(x)}$ for various basic objects (x) of length $\ell^{(x)}$ on a triangular lattice. Colors are associated with different orders $n_s^{(x)}$ of the symmetry axis. For object x, $m^{(x)}$ is the number of first neighboring sites on the lattice.

(x)	Shape	$n_s^{(x)}$	$m^{(x)}$	$\ell^{(x)}$	$\theta_{jam}^{(x)}$	$\theta_p^{(x)}$
(A)		2	8	1	0.9139 (5)	0.4841 (13)
(B)		2	10		0.8362 (7)	0.4611 (9)
(C)		1	10	2	0.8345 (8)	0.4585 (11)
(D)		3	9		0.7970 (4)	0.5214 (9)
(E)		2	12		0.7886 (8)	0.4399 (12)
(F)		1	12		0.7653 (10)	0.4304 (12)
(G)		1	11		0.7739 (7)	0.4815 (11)
(H)		2	12	3	0.7404 (9)	0.4369 (11)
(I)		1	12		0.7226 (6)	0.4461 (5)
(J)		2	10		0.7593 (4)	0.5387 (6)
(K)		6	12	6	0.6695 (7)	0.5836 (11)

used to obtain the dependence of the percolation threshold in polydisperse composites on the dispersion. However, not much is known about the influence of the particle size dispersion on the properties of composite materials and there are still many questions to be answered.

For most real percolating systems, some important physical properties depend on the detailed geometry of the substrate and on the shape and size of the adsorbed particles [27]. Here we present the results of extensive simulations of irreversible deposition of objects of various shapes and sizes on a triangular lattice. Depositing objects are made by directed self-avoiding random walks on the lattice [28] and the percolation thresholds are determined for each type of depositing object. We concentrate here on the influence of shape on the percolation characteristics of the system. Effects of object size on percolation properties are also studied. Furthermore, in order to gain insight into the percolation phenomena in complex systems, simulations are performed for mixtures made of various objects and for polydisperse mixtures containing depositing objects of various sizes. Our recent works [26,29] on how the mixture composition affects the approach to the jamming limit provide a starting point for such exploration.

Section II describes the details of the simulations. Results of the simulations for objects of various shapes and sizes are given in Sec. III. Results for mixtures are also given in Sec. III A. Finally, Sec. IV contains some additional comments and final remarks.

II. DEFINITION OF THE MODEL AND THE SIMULATION METHOD

Our model describes the irreversible deposition of large complex objects onto a substrate. The percolation of nonoverlapping extended objects is investigated using RSA on a two-dimensional (2D) triangular lattice. The depositing objects are made by directed self-avoiding random walks on the lattice. On a triangular lattice, objects with a symmetry axis of first, second, third, and sixth order can be formed. Rotational symmetry of order n_s, also called n_s-fold rotational symmetry, with respect to a particular axis perpendicular to the triangular lattice, means that rotation by an angle of $2\pi/n_s$ does not change the object. For a small number of steps it is easy to find all the shapes that may have different percolation properties. We performed numerical simulations for all such shapes of length $\ell = 1$, 2, and 3, covering two, three, and four lattice sites, respectively. All these objects are shown in Table I. On a triangular lattice it would also be interesting to examine the behavior of a hexagon shown in Table I.

In addition to objects A–K, listed in Table I, percolation properties were investigated for various sizes of basic objects A, C, D, and K. In the case of the dimer (A) and the angled object (C), objects of various sizes are made by repeating each

TABLE II. Illustration of the construction of objects larger than the basic ones. Larger objects are made by repeating each step of the basic object the corresponding number of times. Simulations are performed for ten linear segments (k-mers) of lengths $\ell = 1,2,\ldots,10$; ten angled objects of sizes $s = 1.5,3,\ldots,15$; five triangles of sizes $s = 1,2,\ldots,5$; and five hexagons of sizes $s = 2,4,\ldots,10$.

k-mers		Basic shape (C)		Basic shape (D)		Basic shape (K)	
	$\ell = 1$		$s = 1.5$		$s = 1$		$s = 2$
	$\ell = 2$		$s = 3$		$s = 2$	$\cdots$	$s = 4$
$\cdots$	$\cdots$	$\cdots$	$\cdots$	$\cdots$	$\cdots$	$\cdots$	$\cdots$
$\cdots$	$\ell = 10$	$\cdots$	$s = 15$	$\cdots$	$s = 5$	$\cdots$	$s = 10$

step of a basic shape corresponding number of times. On the other hand, triangles and hexagons of larger sizes occupy all comprised sites on lattice. The construction of larger objects is illustrated in Table II. The size s is taken as the greatest dimension of the object, i.e., as the greatest projection of the object in one of the six directions. Thus the size of a dot is $s = 0$, the size of a one-step walk is $s = 1$, and, for example, the size of the first angled object in Table II is $s = 1.5$ in lattice spacing.

Monte Carlo simulations are performed on a triangular lattice with linear size L up to $L_{\max} = 1000$ sites. Hard boundary conditions are used in the horizontal direction, in which the onset of percolation is detected. This means that, in the horizontal direction, the objects may touch the edge of the lattice but they cannot stick out of it. The periodic boundary conditions are applied in the other directions. The data are averaged over 100 independent runs for each depositing object.

At each Monte Carlo step a lattice site is selected at random. If the selected site is unoccupied, deposition of the object is tried in one of the six orientations. We fix the beginning of the walk that makes the shape at the selected site and search whether all successive ℓ sites are unoccupied. If so, we occupy these $\ell + 1$ sites and place the object. If the attempt fails, a new site and a new direction are selected at random. The coverage of the surface is increased in the process up to the percolation threshold, when a cluster that extends through the whole system appears. We say that a percolating cluster arises in the system when the opposite edges of the system are connected via some path of nearest neighbor sites occupied by the particles. Here we check the connectivity between the left and the right edges of the lattice. The tree-based union and find algorithm was used to determine the percolation threshold [30]. Each cluster of connected sites is stored as a separate tree, having a single "root" site. All sites in the cluster possess pointers to the root site, so it is simple to ascertain whether two sites are members of the same cluster. When a deposited object connects two separate clusters, they are amalgamated by adding a pointer from the root of the smaller cluster to the root of the larger one. This procedure is repeated until the percolation threshold is reached. Another quantity of interest is the jamming limit θ_{jam}, which is reached when no more depositing objects can be placed in any position on the lattice. Details of these simulations are given elsewhere [26,29].

In the case of a mixture, the objects making the mixture are deposited onto the lattice with equal probability. In each deposition attempt one of the objects is selected at random, a lattice site is selected at random, and deposition of the object is tried in one of the six possible orientations. The values of percolation thresholds are determined and the data are averaged over 100 independent runs for each mixture of the objects.

III. RESULTS AND DISCUSSION

It is known [1] that the finite-size scaling theory describes correctly the dependence of the effective percolation threshold θ_p (the mean value measured for a finite lattice) and its standard deviation σ on the linear size L of the lattice. It appears from the scaling theory that the effective percolation threshold θ_p approaches the asymptotic value θ_p^* ($L \to \infty$) via the power law

$$\theta_p - \theta_p^* \propto L^{-1/\nu}. \tag{1}$$

For 2D systems the theoretical value for the correlation length exponent is $\nu = 4/3$. The latter relationship allows us to extrapolate the threshold for an infinite system, $L \to \infty$.

Simulations were performed for lattices of various sizes, ranging from $L = 30$ to $L = 500$ for smaller objects ($s \leqslant 3$) and from $L = 100$ to $L = 1000$ for the largest ones ($s > 3$). Plotting the mean value θ_p of the threshold for various lattice sizes against $L^{-1/\nu}$, we confirm the validity of the finite-size scaling in the system and determine the asymptotic value of the percolation threshold θ_p^*. Finite-size scaling of the lattice

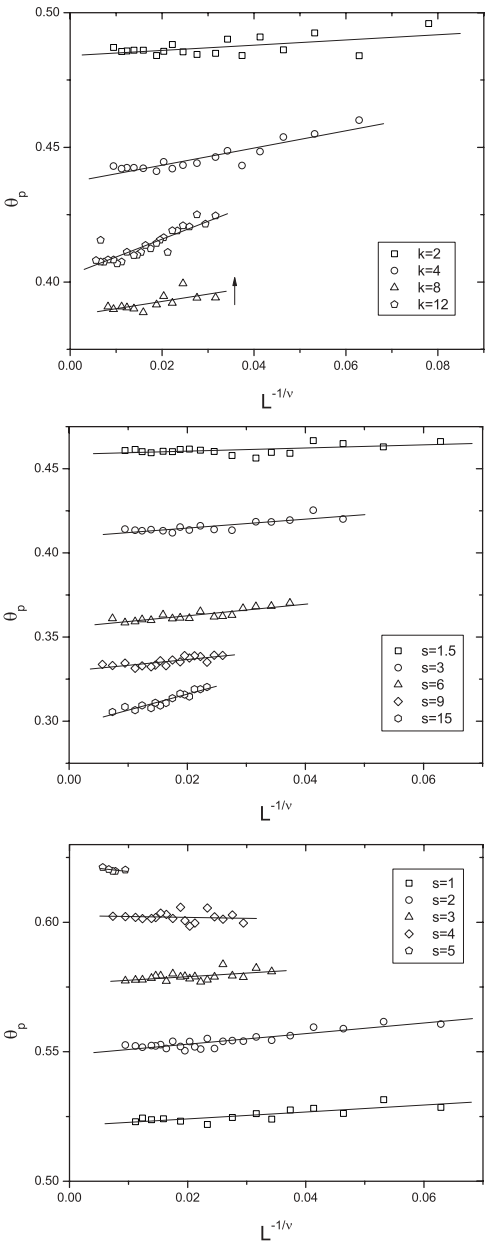

FIG. 1. Finite-size scaling of the percolation threshold θ_p against $L^{-1/\nu}$ with $\nu = 4/3$ for (a) line segments (k-mers) of lengths $\ell = k - 1 = 1, 3, 7, 11$; (b) angled objects (C) of sizes $s = 1.5, 3, 6, 9, 15$; (c) triangles (D) of sizes $s = 1, \ldots, 5$ (see Table II). For clarity, data for $k = 8$ are shifted vertically downward by 0.02.

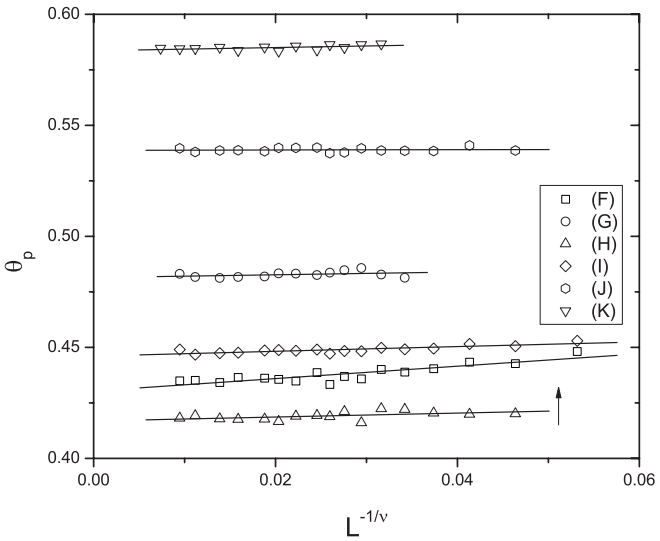

FIG. 2. Finite-size scaling of the percolation threshold θ_p against $L^{-1/\nu}$ with $\nu = 4/3$ for objects H–K from Table I. For clarity, the data for object H are shifted vertically downward by 0.02.

threshold θ_p against $L^{-1/\nu}$ for $\nu = 4/3$ is illustrated in Fig. 1 for k-mers [Fig. 1(a)], angled objects (C) [Fig. 1(b)], and triangles (D) of various sizes [Fig. 1(c); also, see Table II]. Such plots are also shown in Fig. 2 for objects F–K from Table I. Values of the obtained percolation thresholds θ_p^* for various objects are given in Table I together with the corresponding jamming coverages θ_{jam}.

According to the scaling theory the standard deviation σ of the percolation threshold measured for a finite lattice L satisfies the power law

$$\sigma \propto L^{-1/\nu}. \tag{2}$$

In Fig. 3 the standard deviation σ vs L is shown on a double-logarithmic scale for a dimer (A) [Fig. 3(a)], an angled object (C) [Fig. 3(b)], a triangle (D) [Fig. 3(c)], and a hexagon (K) [Fig. 3(d)]. For all objects we obtained confirmation of the power law in Eq. (2), with the value of the exponent $1/\nu$ ranging from 0.714 ± 0.018 to 0.765 ± 0.015. Therefore, apart from a slight deviation for the hexagon (K), these results are in good agreement with the universal value $1/\nu = 3/4$.

Let us first consider the values of percolation threshold for objects E–J in Table I. All of these shapes have the same length, $\ell = 3$. The largest thresholds are observed for objects G and J, while objects E, F, H, and I have significantly lower thresholds (which are in fact very similar to each other). It is obvious that the symmetry order n_s of the shape is not correlated with the percolation threshold for various objects. However, we observe that object J, with the largest threshold, has the smallest number m of the first neighboring sites on the lattice, i.e., $m = 10$. For the second object (G), we have $m = 11$, while for all other objects of length $\ell = 3$, $m = 12$. Shape J is surrounded by the smallest number of neighboring sites and therefore we can say that it is more compact than other shapes of the same length. In addition, among the shapes of length $\ell = 2$, shape D is the most compact ($m = 9$) and therefore has the highest percolation threshold. This strongly suggests that, for various objects of the same length, the percolation threshold

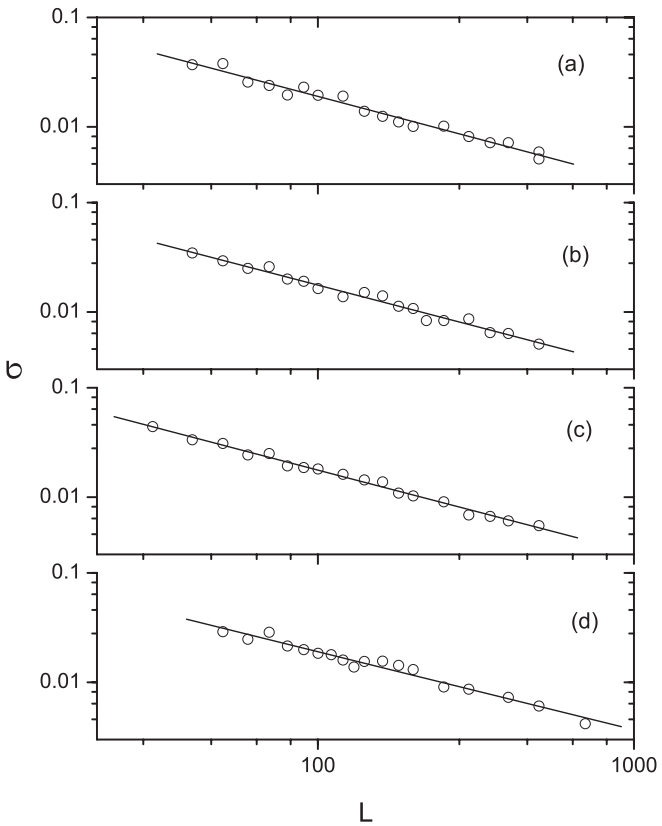

FIG. 3. Standard deviations σ of the percolation threshold on a double logarithmic scale for (a) a dimer (A); (b) an angled object (C); (c) a triangle (D); and (d) a hexagon (K). Straight lines correspond to the best fit according to the power law in Eq. (2) and with the exponents 0.765 ± 0.015, 0.754 ± 0.017, 0.755 ± 0.017, and 0.714 ± 0.018 for objects A, C, D, and K, respectively.

θ_p^* of more compact shapes exceeds the θ_p^* of elongated ones. Qualitatively, we could say that the value of θ_p^* depends on the object's capability to make connections with other depositing objects. The number of nearest neighbors m seems to be a quantity that is closely related to the connectivity, and it is included in Table I. It can be seen that the percolation threshold decreases with m for objects of the same length.

In Fig. 4 the percolation threshold θ_p^* and the jamming θ_{jam}, as well as their ratio $\theta_p^*/\theta_{\text{jam}}$, are plotted against the number k of sites covered by a k-mer. The jamming coverage monotonically decreases with k, while the percolation threshold decreases for shorter k-mers, reaches a value $\theta_p^* \approx 0.40$ for $k = 12$, and, after a smooth minimum, grows for longer k-mers. Consequently, the ratio $\theta_p^*/\theta_{\text{jam}}$ increases. In addition, the inset in Fig. 4 shows that the values of θ_{jam}, as a function of the length of the line segments, decrease according to a power law approaching the asymptotic value $\theta_{\text{jam}}^{\infty} = 0.56 \pm 0.01$. The same kind of dependence was found for the deposition of needles on a square lattice [5,31], but with a different value of $\theta_{\text{jam}}^{\infty}$.

Dependence of the percolation threshold θ_p^*, the jamming coverage θ_{jam}, and their ratio $\theta_p^*/\theta_{\text{jam}}$ on the size s of the angled objects (C) from Table II is shown in Fig. 5. We can

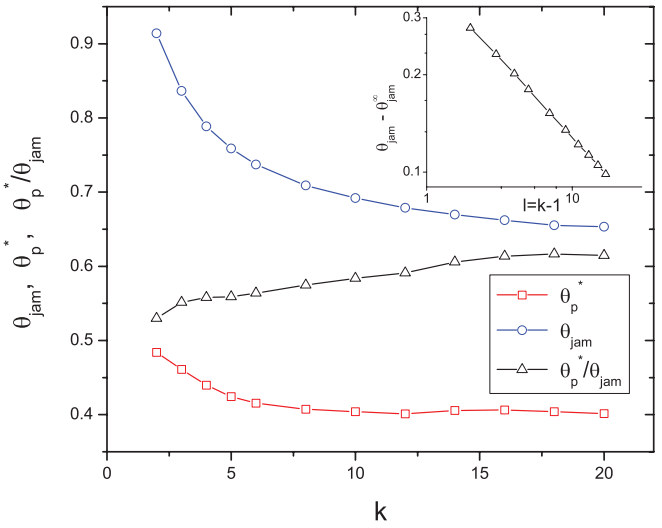

FIG. 4. (Color online) Dependence of the percolation threshold θ_p^*, the jamming coverage θ_{jam}, and their ratio $\theta_p^*/\theta_{\text{jam}}$ on k for k-mers of various lengths ($\ell = k - 1$). Inset: Dependence of $\theta_{\text{jam}} - \theta_{\text{jam}}^{\infty}$ on the length ℓ of the line segments on a log-log scale for $\theta_{\text{jam}}^{\infty} = 0.56 \pm 0.01$. Here and in the following figures, symbols are the actual data and lines are just a guide for the eye.

see that for the angled objects both the jamming coverage and the percolation threshold monotonically decrease with the size of the objects, but their ratio increases. It is interesting that in the case of triangles (D) from Table II the percolation threshold monotonically increases with the size s (see Fig. 6). We observe percolation, especially for large compact objects, very close to the jamming limit. This makes an important difference between the deposition of anisotropic and that of rounder objects on a triangular lattice. The appearance of this unexpected feature is connected with a change in the geometry

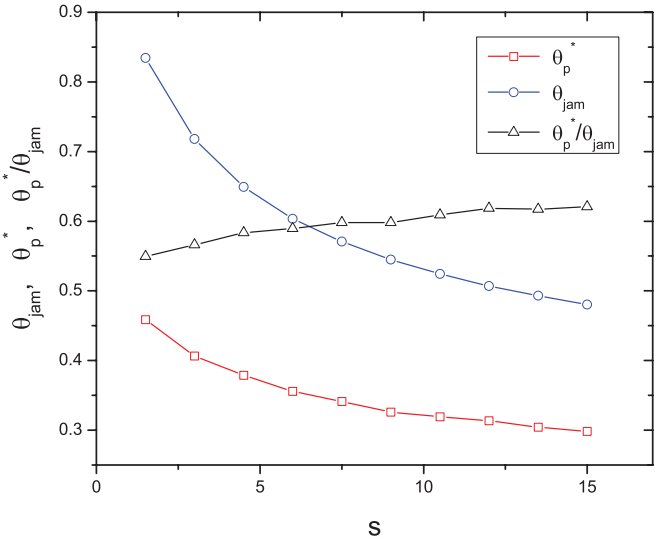

FIG. 5. (Color online) Dependence of the percolation threshold θ_p^*, the jamming coverage θ_{jam}, and their ratio $\theta_p^*/\theta_{\text{jam}}$ on the size s of the angled objects (C). Objects of a larger size are made by repeating each step of a basic shape the corresponding number of times. The size s is taken as the greatest projection of the object in one of the six directions.

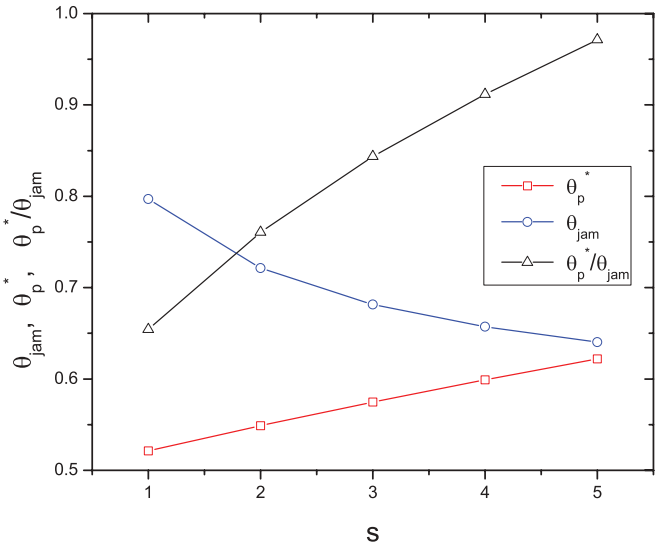

FIG. 6. (Color online) Dependence of the percolation threshold θ_p^*, the jamming coverage θ_{jam}, and their ratio $\theta_p^*/\theta_{\text{jam}}$ on the size s of the triangles (D). Triangles of a larger size also occupy all comprised sites. The size s is taken as the greatest projection of the object in one of the six directions.

of the configurations due to excluded volume effects. Blocking of the substrate area is enhanced by the growth of the k-mer length, making the surface more porous (unoccupied sites can form open and large pores). This results in lower values of percolation thresholds. The porosity of the surface is also responsible for the low values of the percolation thresholds in the case of angled objects, for which there exists a greater probability for blocking the comprised sites. On the other hand, round objects, such as triangles and hexagons, tend to form compact, isolated islands on the lattice. Then the connectivity in the system is poor at low coverages and percolation sets in at larger values of the coverage fraction.

Percolation thresholds θ_P^* vs the length ℓ of the walk that makes the depositing object are given in Fig. 7 for the line

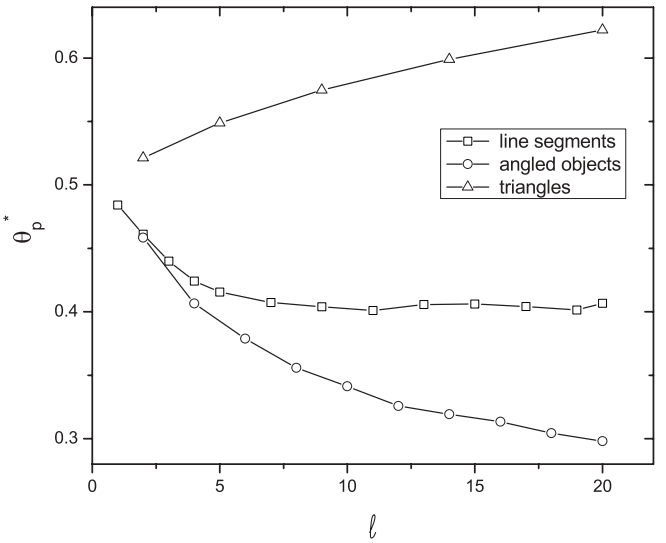

FIG. 7. Dependence of the percolation threshold θ_p^* on the length ℓ of the walks that make the objects.

segments, angled objects, and triangles from Table II. For compact objects, such as triangles, the percolation threshold increases with ℓ. In the case of line segments, θ_p^* decreases with ℓ for shorter lines and, after a smooth minimum at about $\ell = 11$, grows slowly for longer k-mers. Deposition of angled objects is characterized by a relatively high probability for blocking their neighboring sites and the percolation threshold decreases with ℓ. It must be stressed that the difference between the percolation threshold for a compact object and that for an elongated object of the same length increases with their length.

Snapshots of the percolating clusters shown in Fig. 8 can help us to explain qualitatively the behavior of the percolation threshold for various depositing objects. In fact, Fig. 8 shows typical snapshot configurations at the percolation threshold obtained for line segments of length $\ell = 10$ [Fig. 8(a)], angled objects of length $\ell = 10$ [Fig. 8(b)], and hexagons of length $\ell = 6$ [Fig. 8(c)] from Table II. At very early times in the process deposited objects do not "feel" the presence of the others and are adsorbed in any of the six orientations with equal probability. However, in the late stages of deposition the objects must fit into small empty regions, which favors the formation of clusters. Deposition of elongated objects is characterized by domains of parallel objects and large islands of unoccupied sites. A large number of nearest neighbors enhances the connectivity of these objects, and percolation is reached at coverages much lower than the corresponding jamming coverages. On the other hand, compact objects such as hexagons cover the surface more efficiently, at the same time having a lower connecting probability. This results in a percolation threshold close to the jamming limit, while for larger objects percolation cannot be reached.

Compact objects of larger sizes can show a no-percolating behavior. Here we present only the results for the objects and lattice sizes for which, in all $N = 100$ runs, percolation was reached. However, for larger sizes of compact objects such as D, J, and K, a no-percolation regime was observed. This effect is most pronounced for hexagons, for which no percolation was found for objects larger than the basic ones. Speaking to the length of the walks, only basic hexagons (K) of length $\ell = 6$ percolate, while for hexagons of length $\ell = 18$ percolation cannot be reached. The smallest no-percolating objects (J) are made by $\ell = 24$ steps, and the smallest no-percolating triangles (D), by $\ell = 27$ steps. Absence of percolation was not detected for any of the less compact objects considered. These results are in good agreement with the results presented in Ref. [8], where the maximal length for which the most bent particles percolate is $a = 13$, while for particles that are not fully bent the maximal length is about $a = 22$. The absence of percolation has also been reported in studies of RSA of large rectangular particles [32], squares [33], and bent particles [8] on a square lattice.

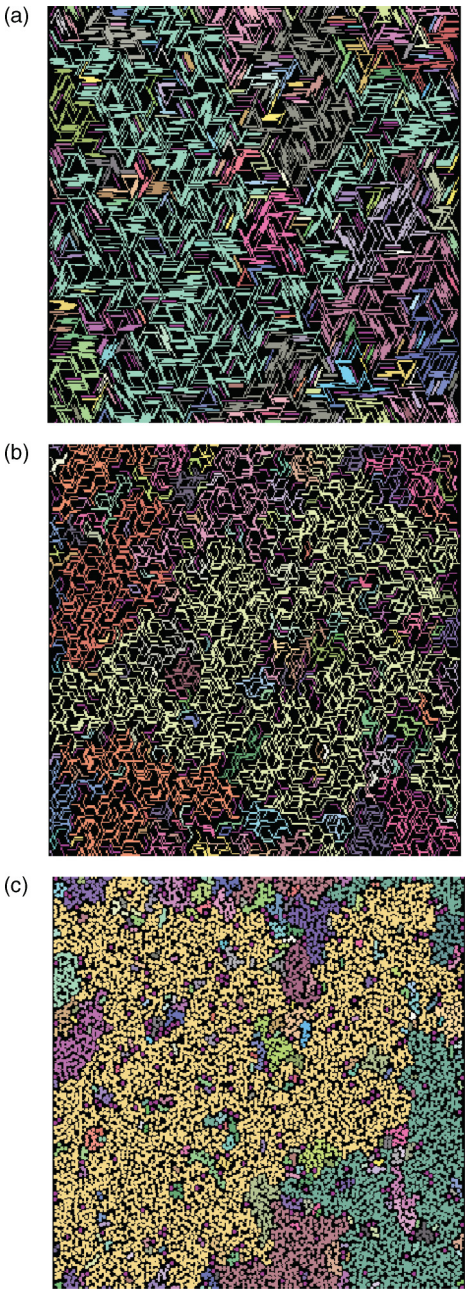

FIG. 8. (Color online) Typical configurations of deposited objects at the percolation threshold for (a) line segments of length $\ell = 10$; (b) angled objects (C) of length $\ell = 10$; and (c) hexagons (K) of length $\ell = 6$ from Table I. Different colors correspond to clusters of connected sites, and the percolating clusters are clearly shown.

A. Percolation in the case of mixtures

RSA of binary mixtures of line segments on a square lattice has been discussed in Ref. [34]. Results of numerical simulations indicate that the mixtures cover the lattice more efficiently than either of the species separately. For binary mixtures of objects of various shapes it was found that this was not always the case [29]. For a number of combinations of depositing objects, including k-mers, the jamming coverage for a mixture has greater values than the jamming coverage for the pure shapes making up the mixture. However, there are also mixtures that have a lower jamming coverage than one of the components. The mutual feature of these mixtures is that the jamming coverages of their components differ significantly.

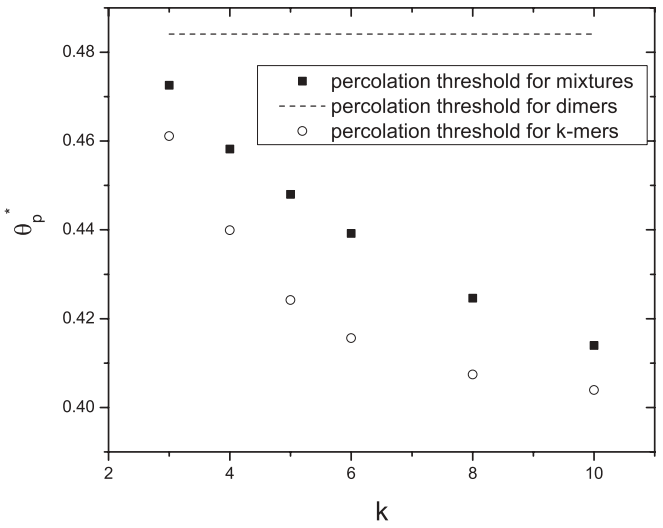

FIG. 9. Percolation threshold θ_p^* for two-component mixtures of dimers and k-mers vs the number of sites covered by the k-mer, $k > 2$ (filled squares). Circles show the percolation threshold for k-mers and the dashed line shows the percolation threshold for dimers.

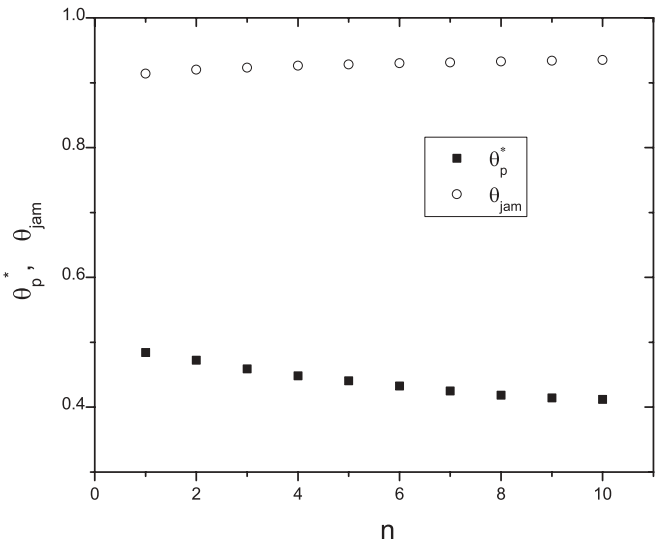

FIG. 10. Dependence of the percolation threshold θ_p^* (filled squares) and the jamming coverage θ_{jam} (open circles) on the number of components n making up the mixture. The number of components in a mixture is always increased by adding a k-mer of a greater length.

In order to examine the percolation properties of mixtures, we performed simulations for two-component mixtures on a triangular lattice. Binary mixtures are made of dimers and k-mers covering various numbers of lattice sites. Results of these simulations are presented in Fig. 9. Percolation thresholds θ_p^* for the mixtures of dimers and k-mers are represented by squares. Circles show the percolation thresholds for k-mers, and the dashed line shows the percolation threshold for dimers. We can see that the percolation threshold for dimers is lowered by adding longer objects. The value of θ_p^* for the mixture decreases with the length of the k-mers combined with dimers, but it is always greater than the percolation threshold for the corresponding k-mer.

Another interesting situation is the combination of no-percolating objects and objects that percolate. For example, when hexagons of sites greater than the basic one are combined with percolating objects, for example, k-mers, the system percolates. We have performed simulations for a large variety of combinations of percolating and no-percolating objects and the system always percolates. The values of the percolation thresholds for the mixtures are greater than the values for the pure percolating shapes.

Effects of polydispesrsity on the percolation properties are studied for mixtures of increasing numbers of k-mers of various lengths. The two-component mixture consists of k-mers covering $k = 2$ and $k = 3$ lattice sites, the three-component mixture is made by adding a k-mer covering $k = 4$ lattice sites, and so on. An n-component mixture contains k-mers covering $k = 2,3, \ldots, n + 1$ lattice sites, and all of them are adsorbed with equal probability. Percolation thresholds are shown vs the number of components n in Fig. 10, together with the corresponding jamming coverages. We can see that for the mixture of k-mers, the percolation threshold decreases with the number of components in the mixture. On the other hand, the jamming coverage increases with n, despite the fact that the number of components is always increased by adding a k-mer of a greater length.

IV. CONCLUDING REMARKS

We have investigated percolation and jamming phenomena for random sequential deposition of objects of various shapes and sizes on a 2D triangular lattice. The shapes are made by self-avoiding lattice steps. A systematic approach is made by examining a wide variety of object shapes and their mixtures.

It has been shown that, for elongated shapes, such as k-mers and angled objects, the percolation threshold monotonically decreases with the size of the objects. However, in the case of more regular and compact shapes the percolation threshold monotonically increases with the object size. We have also shown that the ratio of percolation and jamming thresholds increases with object size for all examined objects. We have pointed out that for various objects of the same length, the percolation threshold of more compact shapes exceeds the percolation threshold of elongated ones. It must be stressed that the percolation thresholds for k-mers deposited on a square lattice [27] exceed the corresponding thresholds on a triangular lattice by $\approx$15% for short k-mers and $\approx$10% for longer ones ($k \geqslant 8$). This difference is due to the orientational freedom of depositing objects. In the square lattice case, the objects can adsorb in four possible directions. On a triangular lattice there are six possible directions for adsorption. Hence, on a triangular lattice there is a greater number of possible orientations and an enhanced probability for the formation of frozen defects of blocked sites.

We have analyzed polydisperse mixtures in which the size of line segments making up the mixture gradually increases with the number n of components. The percolation threshold for a mixture of line segments (Fig. 10) is slightly greater than the percolation threshold of the longest component making the mixture (Fig. 4). For mixtures with a large number of components, i.e., for $n \gtrapprox 7$, this difference is negligible since anisotropic constraints lead to the increased contribution of the longer k-mers in the total coverage fraction of the mixture.

ACKNOWLEDGMENTS

This work was supported by the Ministry of Science of the Republic of Serbia, under Grant Nos. ON171017 and III45016. The work presented was also supported by the Swiss National Science Foundation through SCOPES Grant No. IZ73Z0-128169.

[1] D. Staufer and A. Aharony, *Introduction to Percolation Theory* (Taylor & Francis, London, 1994).
[2] M. Sahimi, *Applications of Percolation Theory* (Taylor & Francis, London, 1994).
[3] M. E. J. Newman and D. J. Watts, Phys. Rev. E **60**, 7332 (1999).
[4] R. Cohen, K. Erez, D. Ben-Avraham, and S. Havlin, Phys. Rev. Lett. **86**, 3682 (2001).
[5] G. Kondrat and A. Pękalski, Phys. Rev. E **63**, 051108 (2001).
[6] F. Rampf and E. V. Albano, Phys. Rev. E **66**, 061106 (2002).
[7] G. Kondrat, J. Chem. Phys. **117**, 6662 (2002).
[8] G. Kondrat, Phys. Rev. E **78**, 011101 (2008).
[9] J. G. Restrepo, E. Ott, and B. R. Hunt, Phys. Rev. Lett. **100**, 058701 (2008).
[10] N. Tsakiris, M. Maragakis, K. Kosmidis, and P. Argyrakis, Phys. Rev. E **82**, 041108 (2010).
[11] V. A. Cherkasova, Y. Y. Tarasevich, N. I. Lebovka, and N. V. Vygornitskii, Eur. Phys. J. B **74**, 205 (2010).
[12] N. I. Lebovka, N. N. Karmazina, Y. Y. Tarasevich, and V. V. Laptev, Phys. Rev. E **84**, 061603 (2011).
[13] R. M. Ziff, Phys. Rev. Lett. **103**, 045701 (2009).
[14] A. S. Ioselevich and A. A. Kornyshev, Phys. Rev. E **65**, 021301 (2002).
[15] N. A. M. Araújo and H. J. Herrmann, Phys. Rev. Lett. **105**, 035701 (2010).
[16] M. Dolz, F. Nieto, and A. J. Ramirez-Pastor, Phys. Rev. E **72**, 066129 (2005).
[17] J. W. Evans, Rev. Mod. Phys. **65**, 1281 (1993).
[18] V. Privman, Colloids Surf. A **165**, 231 (2000).
[19] N. Vandewalle, S. Galam, and M. Kramer, Eur. Phys. J. B **14**, 407 (2000).
[20] P. Adamczyk, P. Romiszowski, and A. Sikorski, J. Chem. Phys. **128**, 154911 (2008).
[21] P. Longone, P. M. Centres, and A. J. Ramirez-Pastor, Phys. Rev. E **85**, 011108 (2012).
[22] P. Meakin and R. Jullien, Phys. Rev. A **46**, 2029 (1992).
[23] B. Bonnier, Y. Leroyer, and E. Pommiers, J. Phys. I **2**, 379 (1992).
[24] N. V. Brilliantov, Y. A. Andrienko, P. L. Krapivsky, and J. Kurths, Phys. Rev. Lett. **76**, 4058 (1996).
[25] Z. Adamczyk, B. Siwek, M. Zembala, and P. Weronsky, J. Colloid Interface Sci. **185**, 236 (1997).
[26] Lj. Budinski-Petković, S. B. Vrhovac, and I. Lončarević, Phys. Rev. E **78**, 061603 (2008).
[27] Y. Leroyer and E. Pommiers, Phys. Rev. B **50**, 2795 (1994).
[28] Lj. Budinski-Petković and U. Kozmidis-Luburić, Phys. Rev. E **56**, 6904 (1997).
[29] I. Lončarević, Lj. Budinski-Petković, and S. B. Vrhovac, Eur. Phys. J. E **24**, 19 (2007).
[30] M. E. J. Newman and R. M. Ziff, Phys. Rev. E **64**, 016706 (2001).
[31] G. Kondrat and A. Pękalski, Phys. Rev. E **64**, 056118 (2001).
[32] M. Porto and H. E. Roman, Phys. Rev. E **62**, 100 (2000).
[33] M. Nakamura, Phys. Rev. A **36**, 2384 (1987).
[34] N. M. Švrakić and M. Hankel, J. Phys. I **1**, 791 (1991).